Catalytic effect of ZnO anchored silica nanoparticles on rubber vulcanization and cross-link formation

*A. Susanna,[a] M. D'Arienzo,[a] B. Di Credico,[a] L. Giannini,[c] T. Hanel,[c] R. Grandori,[b] F. Morazzoni,[a] S. Mostoni,[a] C. Santambrogio,[b] R. Scotti[a]**

[a] Dip. Scienze dei Materiali, INSTM, University of Milano-Bicocca, Via R. Cozzi 55, 20125 Milano, Italy, [b]Dip. Biotecnologie e Bioscienze, University of Milano-Bicocca, Piazza della Scienza, 2, 20125 Milano, Italy, [c]Pirelli Tyre SpA, Viale Sarca 222, 20126 Milano, Italy

ABSTRACT ZnO nanoparticles (NPs) anchored on SiO_2 (ZnO/SiO_2) revealed as activator of higher efficiency in the sulfur crosslinking of isoprene rubber (IR) in comparison with conventional microcrystalline ZnO. The better performance of this innovative catalytic filler has been associated with: i) the faster Zn reaction with stearic acid and curatives, to form the sulfurating complexes at the beginning of the curing process; ii) the faster formation of large amounts of mono- and di-sulfide cross-linking short chains through a breaking-down mechanism of longer poly-sulfide chains, which account for the higher cross-linking density of the final cured material. In the first step of the curing reaction activated by ZnO/SiO_2, the formation of a stearate bridged dimeric zinc complex has been suggested as potential highly reactive intermediate responsible for accelerating the cross-linking reaction.

1. Introduction

Rubber vulcanization is a consolidated chemical process to enhance the mechanical properties of the polymeric material by sulfur cross-linking of the polymer chains [1-3]. Although it seems to be a mature technology at the industrial level, further progresses in research are required, in order to control the sulfur crosslinking reactions and to obtain the best polymer network structure [4].

Furthermore, a design of rubber composites which improves the tire performance, while lowering both energy consumption and CO_2 emission, is strongly requested [5]. For these reasons it appears mandatory to investigate at the molecular level the sulfur cross-link reaction. Several authors studied the curing mechanism by different approaches, kinetic [6, 7], thermodynamic [8-10], mechanic [11, 12], spectroscopic [4, 13, 14]. However, due to the complexity of the reactions between polymer and curing agents and to the difficulty of operating on the rubber matrix by spectroscopic techniques, the reaction pathway still needs to be elucidated. One crucial point is the action of ZnO in association with fatty acids, e.g. stearic acid (STA), in the curing process [12, 15]. Many authors suggested that Zn(II) centers, produced by ZnO interaction with STA, initially form organometallic derivatives with the accelerator molecule N-cyclohexyl-2-benzothiazole sulfenamide (CBS) and then react with sulfur giving polysulfide Zn accelerator complexes, which have a crucial role in the vulcanization reactions. These sulfurating agents react with the rubber polymer to yield a cross-link precursor. [16, 17]. The initial cross-links between the rubber chains generally contain a large number of sulfur atoms, which decrease as the curing reaction proceeds. Although no conclusive evidences of this desulfuration mechanism are reported in the literature, the presence of Zn(II) accelerator complexes was suggested to play a significant role in promoting the formation of short sulfide bridges [16]. Thus, a broad dispersion of Zn (II) centers in the polymer matrix, their efficient combination with the other curatives and their capability to form the sulfur containing complexes are key points for controlling the vulcanization. Moreover, recently the decrease of ZnO amount in rubber curing has become a very urgent environmental issue [18, 19].

In this *scenario*, our group has recently proposed a novel approach to enhance Zn dispersion in rubber and to accelerate the curing reaction [20]. ZnO nanoparticles (NPs) were grown directly on the surface of SiO_2 spherical particles (ZnO/SiO_2), in order to favor the ZnO-SiO_2 interaction, minimizing that among ZnO particles. Thus, ZnO/SiO_2 NPs simultaneously behave as curing agent and reinforcing filler. The immobilization of ZnO NPs on the silica surface, due to covalent Si-O-Zn interaction, provides a homogeneous dispersion of the oxide in the rubber matrix, makes more

available the zinc centers to react with the curatives and increases the efficiency of the rubber curing, lowering the ZnO amount employed in the process [20]. The new material seems promising for industrial applications. Therefore, an appropriate investigation of the ZnO/SiO_2 catalyst as for its action mechanism in the curing reaction is advisable for a better control of the vulcanization process.

The aim of the present work is to study the effect of the silica-supported ZnO NPs on the isoprene rubber (IR) vulcanization, particularly on the formation rate of the sulfurating complexes at the beginning of reaction and of the sulfur cross-links in the final cured material. The study compares the behavior of ZnO/SiO_2 NPs with that of conventional microcrystalline ZnO particles. The curing efficiency of the catalysts was evaluated by the apparent activation energy of the different steps in the process, through a kinetic approach in non-isothermal conditions [21, 22] and using Differential Scanning Calorimetric (DSC) measurements. The reaction products were investigated as for the length of the polysulfide chains responsible for the cross-linking extent of the final cured material, by using the Model Compound Vulcanization (MCV) approach [23, 24]. This consists in the vulcanization of a low molecular weight compound having chemical properties similar to rubber (2,3-dimethyl-2-butene, TME, is a model compound for IR), producing cured compounds which have been analyzed by Mass Spectrometry (MS) [25, 26] and ^{1}H-Nuclear Magnetic Resonance (^{1}H-NMR) spectroscopy [27]. The comparison between the two catalysts has been also discussed on the basis of Fourier-Transform Infrared Spectroscopy FTIR investigation which elucidates some of the intermediate reaction products.

2. Experimental

2.1 Materials

ZnO/SiO_2 synthesis: silica Zeosil MP1165 (BET specific surface area 160 $m^2\ g^{-1}$) was obtained from Rhodia; $Zn(CH_3COO)_2{\cdot}2H_2O$ (99.99 %), NaOH (98 %) and anhydrous ethanol EtOH (99.9%) were obtained from Carlo Erba, Fluka and Scharlau, respectively; Milli-Q water with resistivity > 18.2 MΩ•cm was used.

Preparation of IR nanocomposites: Cis-1,4-polyisoprene rubber (IR) was purchased from Nizhnekamskneftechim Expor; bis(3-triethoxysilylpropyl) disulfide(TESPD) was obtained from Aldrich; antioxidant N-(1,3-dimethylbutyl)-N'-phenyl-p-phenylenediamine (6PPD), Santoflex-6PPD was obtained from Flexsys; the curing agents were purchased as follows: STA (Stearina TP8) from Undesa; N-cyclohexyl-2-benzothiazole sulfenamide (CBS), Vulkacit CZ/C from Lanxess; sulfur Creso from Redball Superfine; ZnO from Zincol Ossidi (wurtzite, specific surface area 5 m^2 g^{-1}).

MCV: TME (≥ 98 %), Water for HPLC and STA (95 %) were obtained from Sigma-Aldrich; Acetronitrile for LC-MS by Chromasolv.

2.2 Synthesis and characterization of ZnO/ SiO_2 NPs

ZnO anchored SiO_2 NPs were prepared according to the previously published procedure [20]. SiO_2 powder (40 mmol) was dispersed in 90 ml of ethanol and sonicated for 10 min (pulses: 1s; 20 kHz). Then $Zn(CH_3COO)_2 \cdot 2H_2O$ (4,05 mmol) and NaOH (12 mmol), dissolved in 30 ml of EtOH, were added under stirring to the SiO_2 suspension, at 65 °C. ZnO NPs formed by hydrolysis and condensation at the silica surface. The loading of ZnO, evaluated by Inductively Coupled Plasma-Atomic Emission Spectroscopy (ICP-AES) according to a previously described procedure [20] is 10.0 weight % corresponding to a reaction yield of 62 %. Hereafter NPs will be labelled ZSO-10.

The presence of crystalline phases was assessed by X-Ray Diffraction (XRD) using a Bruker D8 Advance instrument, with a Cu Kα incident beam (Cu Kα1 λ = 1.5406 Å, Kα2 λ = 1.54433 Å). The morphological characterization of ZSO-10 was performed on a Jeol 3010 High Resolution Transmission Electron Microscope (HR-TEM) operating at 300 kV with a high-resolution pole piece (0.17 nm point to point resolution) and equipped with a Gatan slow-scan 794 CCD camera. Powders were suspended in isopropanol, and a 5 μL drop of this suspension was deposited on a holey carbon film supported on 3 mm copper grid. Reflectance UV-Vis analysis (range 400-200 nm) was performed by a UV Lambda 900 Perkin Elmer spectrometer on powdered samples to

determine the absorption edge energy of ZnO. The absorption onset can be obtained by plotting $\ln 2(I_t/I_0)$ vs. energy [28].

2.3. Preparation of ZnO/ SiO_2 IR nanocomposites (NCs)

NCs with different ZnO content (1.85, 1.20, 0.60, 0.25 parts per hundred rubber, phr) were prepared first by mixing IR with suitable ratios of ZSO-10, SiO_2 Zeosil MP1165 (corresponding to a total amount of 40 phr SiO_2) and TESPT coupling agent (1.2 phr) in a Thermo Haake Reomix lab station internal mixer (250 mL mixing chamber, 0.7 filling factor, 60 rpm) at 140 °C for 3 min.

Then the obtained composites were mixed with the curatives and vulcanized according to the following procedure: i) STA (0.62 phr) and 6PDD (0.48 phr) as antioxidant were added to the composite over 2 min and the sample was mixed for 4 min. at 60 rpm at 140°C; ii) the other vulcanization reactants, i.e. S8 (0.90 phr) and CBS (0.48 phr), were mixed to the compound at 90 °C in a two-roll mill for 3 min; iii) the compound was further molded in the two roll-mill sheets for 2 min to produce sheets of about 2 mm thickness; iv) finally the samples were cured by compression molding in a heating press at 170 °C for 5 minutes at a pressure of 500 N/cm^2, in agreement with the optimum curing time evaluated from the curing profiles of a Moving Die Rheometer (RPA 2000, Alpha Technological).

Hereafter, the cured samples will be called XZSO-IR, where X indicates the ZnO content expressed in phr.

Two reference master batches were also prepared with microcrystalline ZnO for the comparison with XZSO-IR. They were prepared under the same conditions as XZSO-IR by mixing IR with 40 phr of SiO_2 Zeosil MP1165 (Table 1) and adding the microcrystalline ZnO powder (hereafter called C-ZnO) in the first step of vulcanization procedure. The C-ZnO contents were 1.85 and 0.60 phr corresponding, respectively, to the highest and an intermediate loading of the XZSO-IR samples.

Cured reference samples will be labeled as M-XZSO-IR, where M stands for master batch and X indicates the ZnO content expressed in phr. The amounts of filler and ZnO utilized in the vulcanization procedure are reported in Table 1.

Table 1: Filler and ZnO loading of XZSO-IR and M-X ZSO-IR NCs (in phr)

Samples	ZnO	Filler and activator composition			
		IR	SiO_2	ZSO-10	C-ZnO
1.85ZSO-IR	1.85	100	23.35	18.50	-
1.20ZSO-IR	1.20	100	29.20	12.00	-
0.60ZSO-IR	0.60	100	34.60	6.00	-
0.25ZSO-IR	0.25	100	37.75	2.50	-
M-1.85ZSO-IR	1.85	100	40.00	-	1.85
M-0.60ZSO-IR	0.60	100	40.00	-	0.60

2.4. Swelling experiments

Swelling experiments were performed on XZSO-IR and M-XZSO-IR to evaluate the cross-linking degree. Samples of 10 x 10 x 2 mm^3 (0.20 ± 0.02 g) were immersed in closed vessels filled with 10 mL of toluene at 25°C for seven days in the dark to avoid photo-degradation reactions. Toluene was replaced daily with fresh solvent to eliminate all the extracted fractions. Finally, the swollen mass was weighted and dried to constant mass in vacuum at 70°C for 12 h. The volumetric fraction of the swelled rubber V_r was calculated according to the following equation [29]:

$$V_r = \frac{(m_d - f m_0)\cdot \rho_p^{-1}}{(m_d - f m_0)\cdot \rho_p^{-1} + m_{so}\cdot \rho_s^{-1}} \qquad (1)$$

where m_0 is the weight of the composite before swelling; m_d the weight of the dried mass after swelling; $m_{so} = (m_{sw} - m_d)$ the weight of the solvent in the swollen mass; m_{sw} the weight of the swollen mass; $\rho_p = 0.94$ g•cm^{-3} is the IR density; $\rho_s = 0.87$ g•cm^{-3} is the toluene density; f is the fraction of the filler in the composites as determined by TGA. The cross-link density ν, the number of network chains per gram bounded on both ends by crosslinks, was calculated according to the Flory-Rehner equation [30];

$$\nu = \frac{[\ln(1-V_r) + V_r + \chi V_r^{\,2}]}{-2\cdot \rho_p \cdot V_s \cdot (V_r)^{1/3}} \qquad (2)$$

where V_s=105.91 is the molar volume of toluene and χ is the Flory solvent-polymer interaction term [31], which is 0.43 for toluene-IR [32].

2.5. Apparent Activation Energy of curing process from Differential Thermal Analysis

The curing process of the IR composites was studied by a kinetic approach using the DSC analysis, carried out on a DSC Mettler Toledo Star Thermal Analysis System, equipped with a N_2 cooling apparatus, at different heating rates: 5, 10 and 20 °C/min. In particular, the apparent activation energy E_α of the different steps of vulcanization was evaluated from the exothermic curing peak of the DSC thermograms (Figure 1a) according to the method developed by Kissinger [33] and the kinetic model proposed by Vyazovkin [22].

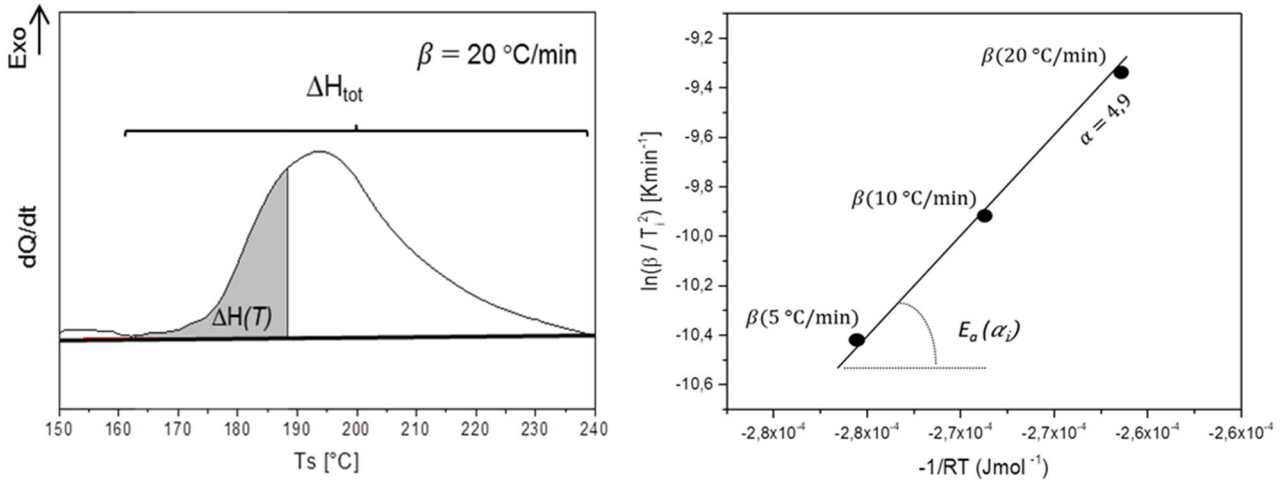

Figure 1: a) Exothermic curing peak from DSC thermogram; b) Plot of ln β/T_i^2 vs $1/T_i$ for a selected value of conversion degree α; heating rates β, and the activation energy E_α calculated as slope are also indicated. (Examples related to sample 1.85 ZSO-IR)

The model is based on the assumptions that i) E_α depends on the conversion degree (α) of the reaction; ii) at fixed value of α, E_α is the same whatever the used heating rate (β).

According to this model, the value of α is:

$$\alpha = \frac{\Delta H(T)}{\Delta H_{tot}} \qquad (3)$$

where $\Delta H(T)$ is the integral of the exothermic peak from the starting vulcanization temperature T_o to the temperature T and ΔH_{tot} is the integral of the total vulcanization peak (Figure 1a). The kinetic equation of the vulcanization process is:

$$\frac{d\alpha}{dt} = k(T)f(\alpha) \qquad (4)$$

where $k(T)$ is the constant rate and $f(\alpha)$ is a functional form of the degree of vulcanization which depends on the reaction mechanism. As $\beta = dT/dt$, equation (4) can be rewritten at constant β as:

$$\frac{d\alpha}{dT} = \beta^{-1}k(T)f(\alpha) \qquad (5)$$

Substituting $k(T)$ in (5) according to the Arrhenius equation (A is the pre-exponential factor, R the gas constant) and integrating over T:

$$g(\alpha) = A\beta^{-1}\int_{T_0}^{T} e^{(-\frac{E_a}{RT})}dT \qquad (6)$$

where $g(\alpha) = \int_0^{\alpha} d\alpha/f(\alpha)$.

Solving the integral (6) [34] at fixed values of α (iso-convertional or free-kinetics model [22, 35]), the following equation is obtained

$$ln\frac{\beta}{T^2} = ln\frac{RA}{E_a} - \frac{E_a}{RT} \qquad (7)$$

According to equation (7), for each value of α, the linear plot of $\ln(\beta/T^2)$ *vs* $1/T$ enables E_α to be determined from the slope (Figure 1 b).

2.6 Model compound vulcanization

MCV experiments were performed by curing TME as model compound in the presence of 18.50 phr of ZSO-10, corresponding to 1.85 phr of ZnO (sample ZSO-TME) or of 1.85 phr C-ZnO powder (sample C-ZnO-TME). The amounts of the other curatives are: 2 phr of STA, 1.6 phr of CBS, 3 phr of sulfur. Curing reactions were performed in a 5 ml closed conical vial, heated in an oil bath at 120 °C for different times (5, 10, 20 min). After the reaction, the vial was cooled down in a liquid nitrogen bath and the reaction mixture was filtered several times by using a 2 µm porous filter. The reaction products were determined by MS and ^{1}H NMR.

MS experiments were performed at different reaction times on cured samples diluted in acetonitrile (1:10 vol:vol). The spectra were acquired in positive-ion mode on a Q-Star Elite instrument (AB Sciex), equipped with a nano-electrospray ion source and a time-of-flight analyzer, employing the following instrumental setting: scan range 50-450, declustering potential 60 V, curtain gas 20 PSI and ion spray 1.1 kV. Relative quantification of the species at different reaction times was performed by adding an internal standard at fixed concentration before MS analysis (diethylamine, c = 48 μM) and normalizing peak intensities according to the standard signal.

^{1}H NMR spectra were recorded at 500 MHz on samples dissolved in $CDCl_3$ (1:10 vol:vol). Chemical shifts were determined relative to the residual solvent peak ($CDCl_3$, δ 7.26 ppm).

2.7 FTIR Spectroscopy

FTIR analysis was performed to investigate the reactivity of ZnO with the STA and the subsequent reaction with the activator CBS and sulfur.

The reaction was carried out at 120 °C: i) in the presence of TME as model compound following the sequence of mixing ZSO-10 or C-ZnO with STA, then CBS and finally sulfur; ii) in the solid state without TME following the same mixing sequence and adding the curatives directly to ZSO-10 or C-ZnO, in order avoid the superimposition of TME signal on the FTIR spectra; iii) in $CHCl_3$ to confirm the reactivity of ZSO-10 or C-ZnO with the curatives without TME. The relative amounts of reagents are the same reported in the recipe of paragraph 2.6. Samples were put in a closed vessel or in a conical vial heated at 120 °C for 20 minutes, then quenched in liquid nitrogen to stop the reaction before recording FTIR spectra at room temperature. The analysis was performed with a Perkin Elmer Spectrum 100 instrument by a single reflection Attenuated Total Reflection (ATR) method (1 cm^{-1} resolution spectra, 650-4000 cm^{-1} region, 16 scans).

3. Results and discussion

3.1 Characterization of ZnO/ SiO_2 NPs

Although already reported in a previous paper [20], the morphological and structural characterizations of ZSO-10 were repeated and here shown, in order to discuss why ZnO NPs

anchored to SiO_2 affect the curing process. TEM image of ZSO-10 (Figure S1 in Supporting Information) showed that silica NPs (size 20-30 nm) are decorated by spherical ZnO NPs (average diameter 4-6 nm). HRTEM demonstrated that ZnO NPs are amorphous, in agreement with XRD patterns. Previous results were also confirmed by the UV-Vis absorption spectra of ZSO-10 which showed an energy blue-shift (Eg =3.38 eV) compared to bulk ZnO (Eg = 3.29 eV) [28, 29], attributable to the smaller NPs dimension.

3.2. Vulcanization of ZnO/ SiO_2 IR NCs

The vulcanization curves for XZSO-IR and M-XZSO-IR NCs confirmed the results reported in our previous study [20]. All XZSO-IR samples showed values of maximum torque (MH) higher than those of M-XZSO-IR containing comparable amounts of ZnO (See Table S1 in Supporting Information). These outcomes demonstrate a better curing efficiency in the presence of ZSO-X NPs compared to the conventional curing process [20], which uses microcrystalline ZnO.

Swelling experiments were also performed to evaluate the cross-link density (ν) of cured NCs, according to the Flory-Rehner equation (2). The values for XZSO-IR and M-XZSO-IR samples are reported in Figure 2 at different ZnO loadings.

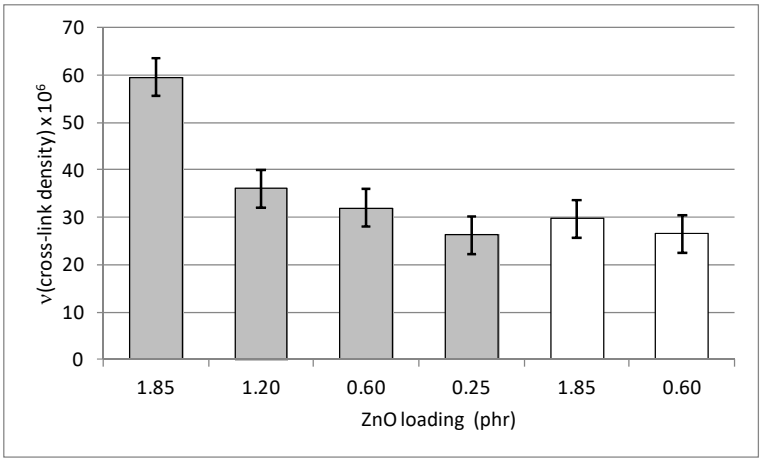

Figure 2: Cross-link density of cured XZSO- IR (grey) and M- XZSO- IR (white) NCs

The results demonstrate that in the investigated range of compositions, the reticulation degree increases with the ZnO content in both series of NCs. However, XZSO-IR show cross-link densities

higher than M-XZSO-IR, in the presence of comparable loadings of ZnO. This is in agreement with the better curing efficiency of ZSO-X compared to C-ZnO.

3.3 Apparent Activation Energy of curing process from Differential Thermal Analysis

The vulcanization processes of XZSO-IR and M-XZSO-IR were studied by a kinetic approach in non-isothermal conditions, using DSC at different heating rates (5, 10 and 20°C/min). As a representative example, DSC profiles of 1.85 ZSO-IR and M-1.85 ZSO-IR at 5 °C/min are shown in Figure 3 a and b, respectively.

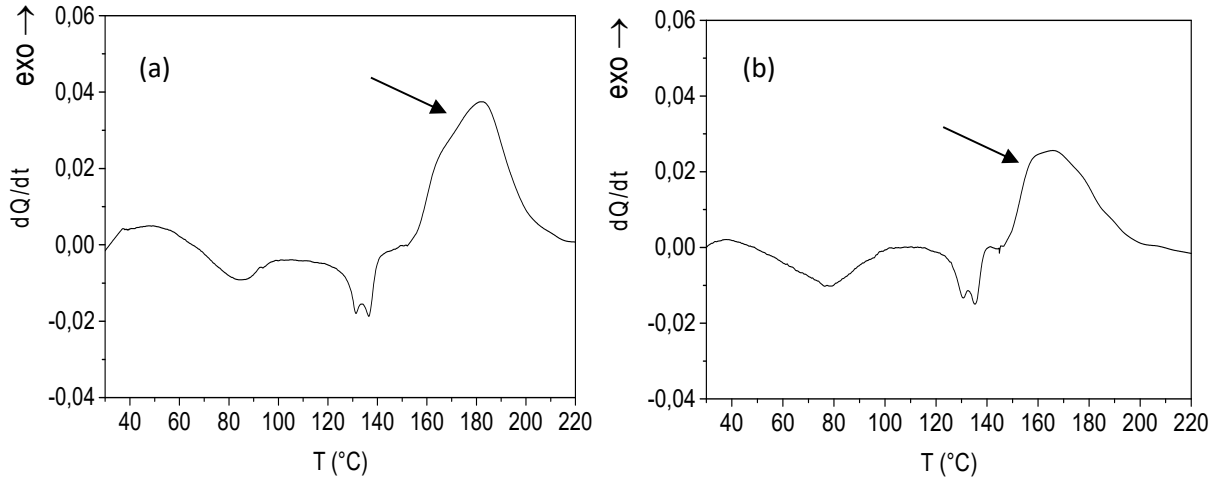

Figure 3: DSC profiles of a) 1.85 ZSO-IR and b) M-1.85 ZSO-IR at 5 °C/min heating rate. The arrows indicate the exothermic peaks of the vulcanization process.

Both NCs show three endothermic peaks: at ~ 80 °C (melting point of STA), at 130 °C (partial reversion of polymeric sulfur to the molecular form) and at 136°C (melting point of polymeric sulfur). Furthermore, at T > 140 °C the exothermic bell-shaped peak due to the vulcanization process can be observed.

This vulcanization peak includes the enthalpy contributions of all the reactions involved in the sulfur curing process in the presence of activators and accelerators. According to the more

recognized hypothesis in the literature [12, 15-17], the main stages of this process are outlined in Scheme 1.

Scheme 1: main stages of the vulcanization process [12, 15, 17]

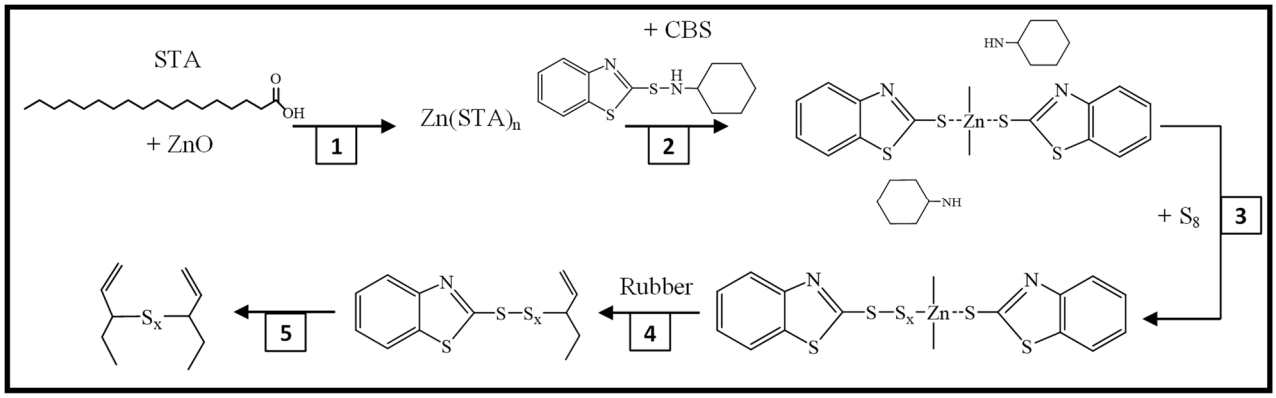

Although it is not possible to distinguish the enthalpy of the single steps, it can be assumed that the vulcanization peak consists of three main regions at increasing α values [36, 37]: i) the induction period at the beginning of the process, where the activator and the accelerator react with sulfur forming the sulfuring complex (stages 1-3 in the Scheme 1) and in turn with the rubber chains giving the cross-link precursors (stage 4); ii) the curing period, in which the cross-link precursors react with the rubber chains leading to the formation of the sulfide network (stage 5) and iii) the overcuring period, which involves the last vulcanization reactions of the polymer and phenomena of reversion due to the breakdown of some unstable polysulfide cross-links.

The apparent activation energy E_α was calculated at different α from the linear plot of ln β/T^2 *vs* 1/T according to equation (7). The variation of E_α vs α of all XZSO-IR and M-XZSO-IR samples are reported in Figure 4.

The trends of E_α are very different in the two cases whatever the ZnO loading. In fact, in the induction period the values of E_α of XZSO-IR are much lower than those of M-XZSO-IR.

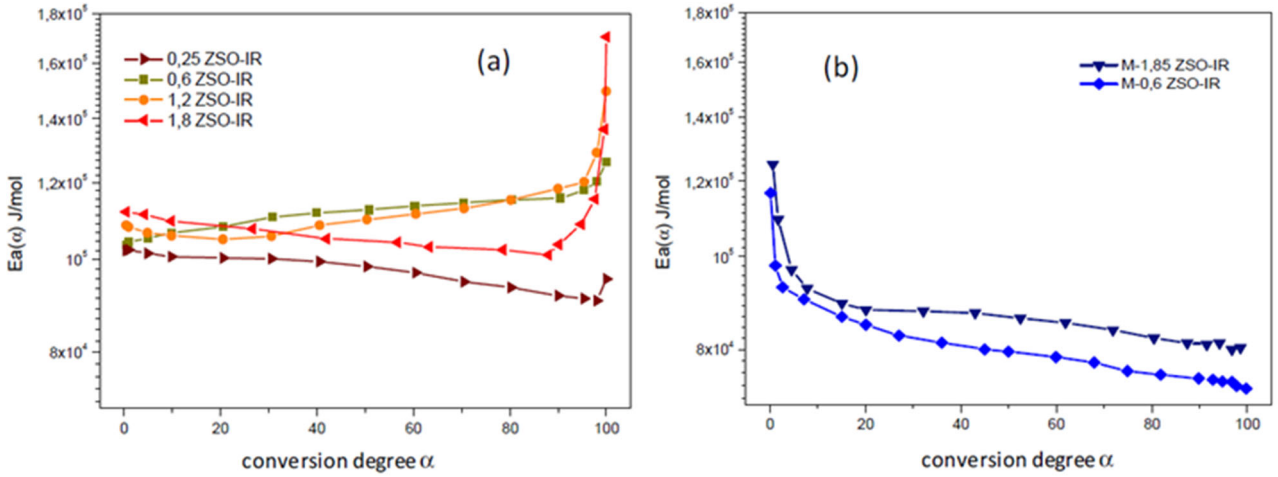

Figure 4: Plots of the apparent activation energy E_α *vs* the conversion degree α calculated by equation (7) of a) XZSO-IR and b) M-XZSO-IR NCs

During the curing stage, E_α values remain stable in both cases; in the last curing step the two processes show an opposite trend, since the E_α values of XZSO-IR remarkably increase while those of M-XZSO-IR decrease. These results demonstrate that, at low conversion degrees, the first steps of the curing process (reaction of ZSO-10 with STA and formation of the sulfuring zinc complex with CBS and sulfur) seem more accelerated compared to the curing process in the presence of C-ZnO.

Besides, the highest E_α in the last stage of XZSO-IR curing suggests that further reactions of the crosslinked rubber (i.e. overcuring) seem to be more difficult than in M-XZSO-IR. Both these indications will be related to the better efficiency of the curing promoted by ZnO-10 and will be further discussed in the following sections.

3.4 Model compound vulcanization

The catalytic mechanism involving ZnO/SiO_2 (ZSO-10 sample), and in particular their effect on the formation of the sulfur cross-links, was investigated in the vulcanization of TME, analyzing the reaction products after 5, 10 and 20 minutes at 120°C by MS and ^{1}H-NMR and comparing them with the results obtained using C-ZnO under the same reaction conditions. In Figure 5 the MS spectra, obtained operating in positive mode, of the ZSO-TME and C-ZnO-TME reaction products

are shown. Spectra were recorded after 5 minutes of the curing process (MS spectra after 10 and 20 minutes are reported in Figure S2 of Supplementary Information).

The MS spectra of these samples show signals that can be attributed to two series of compounds: i) the accelerator CBS (m/z=265) and its by-products (step 2 in Scheme 1) from the curing reactions: cycloexylamine (CHA, m/z=100); a recombination product of mercaptobenzothiazole (MBT) and CHA (m/z= 233) and the MBT dimer (m/z= 332); ii) the cured products of the MCV constituted by two molecules of TME crosslinked by poly- or mono-sulfide chains, TME-S_x-TME with x=1-8 (m/z = 198, 230, 262, 294, 326, 358, 390, 422 for, respectively, x = 1-8). The MS signals due to each TME-S_x-TME species show the presence of two additional peaks, corresponding to the partial oxidation of the TME units during the cross-linking reactions and the formation of one or two 2,3-dimethylbutadiene units instead of the TME molecules (with the loss of 2 or 4 Da, respectively) [38]. The identification of the TME-S_x-TME species was also confirmed by MS/MS experiments, with the detection of the TME ion upon collision-induced dissociation (CID) (Figure S3 in Supporting Information). Hereafter, the formula TME-S_x-TME stands for the sum of the three species with the same length of polysulfide chains S_x.

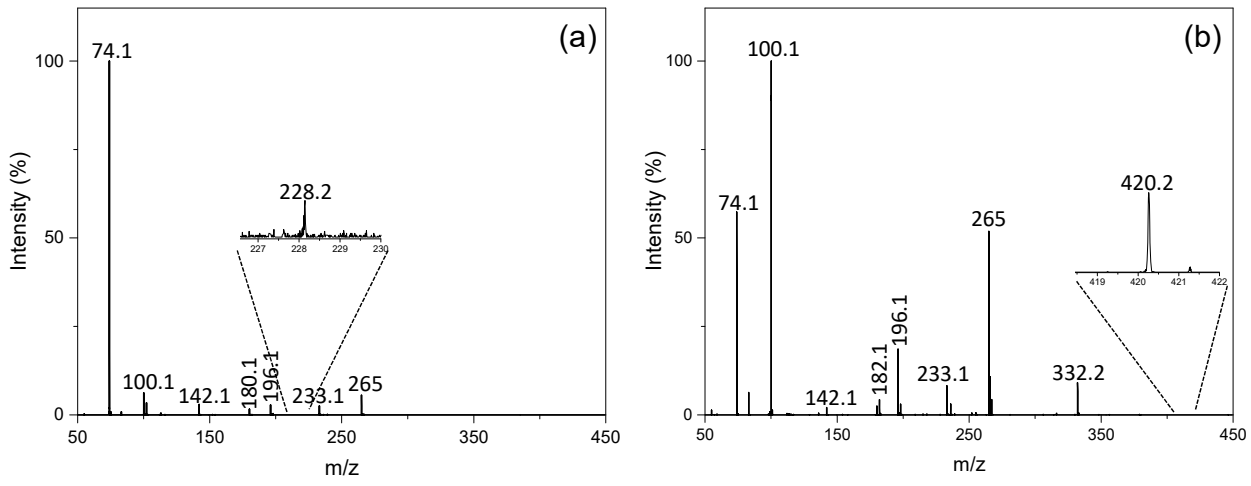

Figure 5: MS spectra of a) ZSO-TME and b) C-ZnO-TME curing products after 5 minutes of reaction at 120°C.

The relative amount of TME-S_x-TME species at different reaction times (5, 10, 20 min) for ZSO-TME and C-ZnO-TME cured at 120°C was determined by quantification of the MS peaks relative to the diethylamine internal standard (see 2.6 paragraph). The plots are reported in Figure 6.

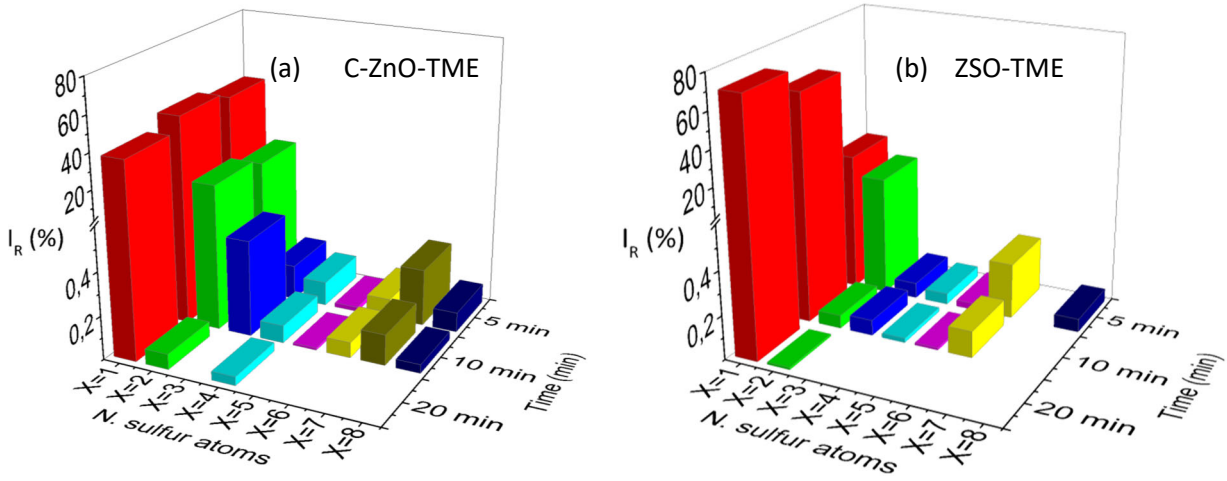

Figure 6: Relative amount of TME-S_x-TME (x=1-8) detected by MS as a function of reaction time of a) C-ZnO-TME and b) ZSO-TME both cured at 120°C.

In both samples, at the lowest tested curing time (5 min) a distribution of mono-, di- and polysulfide TME-S_x-TME products is present with a considerable contribution of long polysulfide chains (S_x with $x \geq 4$). Increasing the curing time, the length of the polysulfide chains progressively decreases and the mono-sulfide species TME-S-TME become the almost unique products.

The comparison between the two systems demonstrates the overall faster reactivity of ZSO. In fact, it is evident that for ZSO-TME i) the amount of poly-sulfide chains (S_3-S_8) is always lower than for C-ZnO-TME, already after 5 min of curing reaction; ii) the progressive formation of mono-sulfide chains starting from the longest poly- and di-sulfide species, is faster; iii) already after 10 min, the amount of mono- sulfide is higher.

The MCV products observed for ZSO-TME and C-ZnO-TME were also studied by ^{1}H NMR, by comparing the spectra with those of known reference compounds [27], in order to confirm the

identification of the cured compounds by MS. Figure 7 shows the ^{1}H NMR spectra (range 3.5-5.6 ppm) of the ZSO-TME and C-ZnO-TME products obtained at 120 °C after 10 minutes as a significant example (Complete ^{1}H NMR spectra of ZSO-TME and C-ZnO-TME are reported in Figure S4 in Supporting Information).

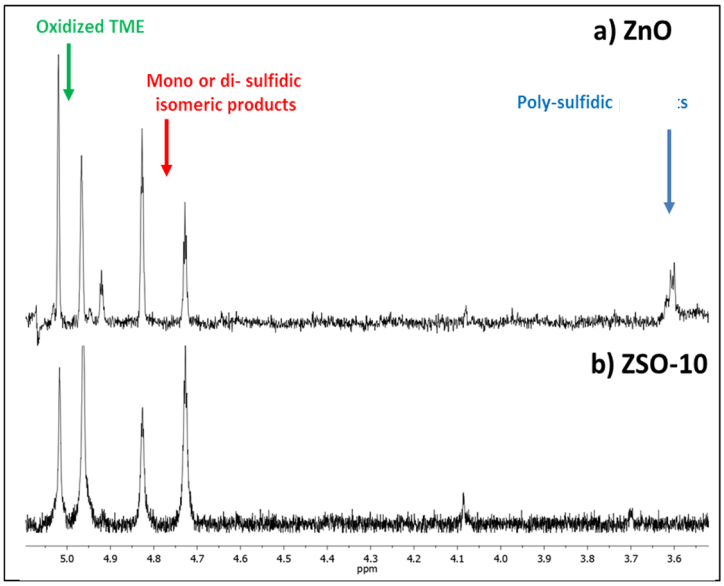

Figure 7: ^{1}H NMR spectra of (a) C-ZnO-TME and (b) ZSO-TME after 10 minutes of reaction at 120 °C

The ^{1}H NMR spectrum of C-ZnO-TME (Figure 7 a) displays the presence of poly-sulfide products. In fact, the chemical shifts in the range of 3.7-3.4 ppm correspond to TME-S_x-TME products with $x > 3$. No signal of the monosulfide TME-S-TME at 3.15 ppm is detectable. However, the signals at 4.73 and 4.83 ppm can be related to the formation of isomeric crosslinked TME mono- or di-sulfide products, which form via allylic substitution during the curing process [27]. Moreover, signals at 5.07 and 4.97 ppm may be associated to a partial oxidation of TME and to the formation of 2,3-dimetylbutadiene [38].

The ZSO-TME ^{1}H NMR spectrum (Figure 7 b) evidences at 4.73 and 4.83 ppm the peaks associated to the isomeric crosslinked TME mono- or di- sulfide products, which are larger than in C-ZnO-TME (. On the other side, the peaks due to poly-sulfide TME-S_x-TME products are almost

undetectable, due to the lower amount of TME-S_x-TME products with x > 3 and the complete absence of S_7 and S_8 chains, as indicated by MS analysis.

In conclusion, the results of the MCV confirm that, in the sulfur vulcanization process, the production of short sulfide chains is due to a breaking-down mechanism of the longer poly-sulfide chains formed at the beginning of the cross-linking reaction. This is in agreement with the reaction sequence for the cross-linking formation proposed in the literature [39] (Scheme 2) where Zn(II) centers promote the S-S breakage through their coordination to the cross-linking precursor. In particular, the linkage of Zn(II) center with a sulfur atom of the polysulfide chain distant from the accelerator molecule weakens an S-S bond close to the rubber, shortening the part of the chains S_y linked to rubber [39]. MS results assess that this sequence can be repeated more than one time, progressively shortening the polysulfide chains. Zn(II) centers were also proposed [40] to break-down the already formed polysulfide cross-links through the formation of an intermediate adduct between zinc sulfurating complex and sulfidic chains.

Scheme 2: mechanism of the cross-linking reaction

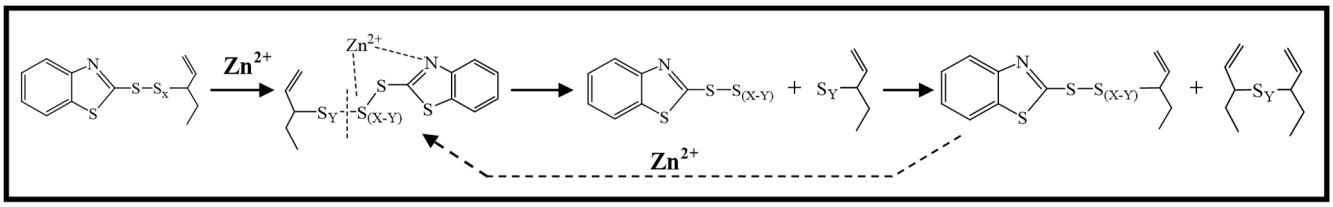

The MCV results also highlight that ZSO-TME and C-ZnO-TME samples with different ZnO morphology and size follow different curing reaction paths. In fact, in the presence of the well distributed ZSO-10 NPs linked on the silica surface, the desulfuration mechanism of the long poly-sulfide chains (S_3-S_8) to give the shortest sulfide chains (S_1, S_2) is faster than in the presence of microcrystalline C-ZnO. Considering the previous mechanisms (Scheme 2), these suggest that in the presence of ZSO-10 NPs the zinc intermediate complexes more easily form and are more available to further react and coordinate the polysulfide in the curing stage, than with C-ZnO.

This is in agreement with the higher cross-linking density of XZSO-IR calculated by the Flory-Rehner equation and can be related to the kinetics investigation, which demonstrates that the E_α values in the induction vulcanization step are lower in the presence of ZSO-10 compared to C-ZnO, thus promoting a more efficient vulcanization.

Moreover, the high E_α values in the last step of ZSO-TME curing may be attributed to the larger amount of stable mono- and di-sulfide crosslinking chains obtained in the presence of ZnO-10 than for C-ZnO, which may effectively hinder the overcuring process.

3.5 FTIR analysis of ZnO

FTIR analysis was performed on both ZSO-TME and C-ZnO-TME to investigate the interaction of ZnO with STA and the successive reactions with CBS and sulphur (Stages 1-3 in Scheme 1). In figure 8, the ATR-FTIR spectra of ZSO-TME before and after the reaction with STA are reported in comparison with the spectra of bare silica, in the range 800-1300 cm^{-1}.

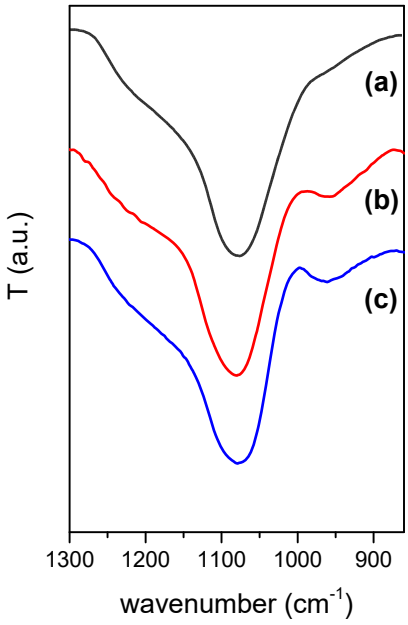

Figure 8: ATR-FTIR spectra of ZSO-TME a) before and b) after the reaction with STA at 120°C; c) bare SiO_2.

As discussed in the previous paper [20], the band at 954 cm^{-1} attributed in bare SiO_2 to –Si-OH stretching vibration [41] (Figure 8 c) shifts to higher frequency and becomes a shoulder at ~ 965

cm^{-1} in ZnO-10 (Figure 8 a), due to the co-presence of –Si-OH and of the symmetric Si-O-Zn stretching vibration [42-44]. After reaction with STA the band at 965 cm^{-1} turns back to 954 cm^{-1} (Figure 8 b).

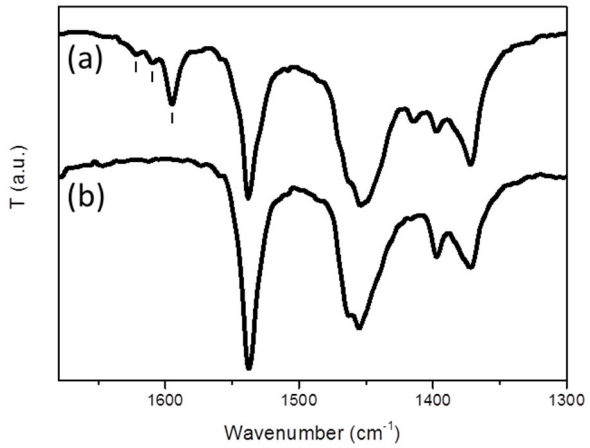

Figure 9: ATR-FTIR spectra of a) ZSO-TME and b) C-ZnO-TME (right) after reaction with STA at 120°C.

This indicates that the surface silanol groups are restored and suggests that the zinc anchored to silica NPs was released after reaction with STA. The ATR-FTIR spectrum of ZSO-TME after the reaction with STA is reported also in the range 1300 -1680 cm^{-1} in comparison with this of C-ZnO-TME (Figure 9).

Both spectra show at 1538 cm^{-1} and 1398 cm^{-1} the stearate antisymmetric and symmetric stretching vibrations [45] attributed to zinc distearate, which contains four bridging carboxylate groups coordinated to Zn(II) [46] (FTIR spectrum of pure zinc stearate is reported in Figure S5 of Supporting Information as a comparison). Surprisingly, ZSO-TME shows additional vibrations both in the region of the antisymmetric carboxylate stretching and of the symmetric one, respectively at 1596, 1614, 1625 cm^{-1} and at 1416 cm^{-1}. Other possible absorption bands in the region of symmetric vibrations may be hidden by the superimposition with the -CH_2- scissoring vibration at 1464 cm^{-1} and of the C-H_2 bending at 1454 cm^{-1}.

In order to study the reactivity of the ZnO particles of ZSO-10 and C-ZnO samples towards STA avoiding the superimposition of the TME signals on the FTIR spectra, the experiments were repeated in another solvent ($CHCl_3$) instead of TME. The results confirmed the same reactivity of ZSO-10 and C-ZnO and the formation of the same different carboxylate species as detected in TME (Figure S6 a, d, in Supporting Information). The experiment was also performed by reaction of STA with solid ZSO-10 and C-ZnO without TME; also in this case the same carboxylate bands were observed for both samples. Moreover, in ZSO-10, in the absence of the alkyl groups signals of TME, another band attributable to a symmetrical stretching mode of the stearate was detected at 1434 cm^{-1} (Figure S7 in Supporting Information).

The differences between the wavenumbers of the antisymmetric and symmetric modes of the carboxylate units are related to the kind of their coordination and for both ZSO-TME and C-ZnO-TME they agree with those reported for a bridging coordination between two metal centers [47].

In a recent work, Ikeda et al. [42] deeply investigated the interaction of zinc with STA under vulcanization conditions. They demonstrated by experimental and computational approaches, that, at high temperature (140°C), the complex $(Zn_2(\mu\text{-}O_2CC_{17}H_{35})_2)^{2+}\cdot 4Y$ formed, having 1:1 Zn: stearate molar ratio and roughly tetrahedral Zn coordination. Its structure was postulated as two carboxylate groups bridging two Zn(II) centers and the Y groups (OH^-, water and/or rubber segment) completing the Zn coordination (Figure 10) [43, 44].

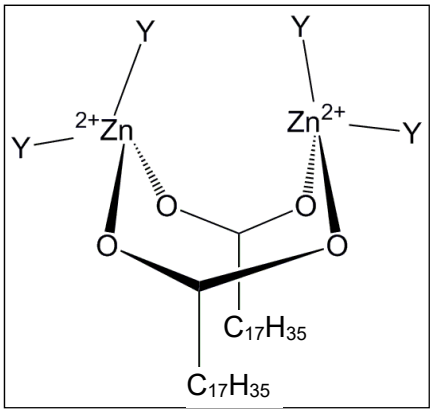

Figure 10: Proposed structure of the bridging bidentate complex $(Zn_2(\mu\text{-}O_2CC_{17}H_{35})_2)^{2+}\cdot 4Y$ from ref. [42].

These authors also showed by DFT calculations that, depending on the Y groups, the complexes present different carboxylate vibrations. In particular the most stable species identified by Ikeda has the antisymmetrical stretching at 1596 cm^{-1} and the symmetrical one at 1434 cm^{-1}. This complex was suggested, based on energy evaluation, as probable intermediate in accelerating the sulfur cross-linking reaction of rubber.

The vibrational bands at 1596 and 1434 cm^{-1} we observed in ZSO-TME after reaction with STA, perfectly agree with those of the stearate bridged species suggested by Ikeda [42]. The less intense bands at 1614, 1625 and 1416 cm^{-1} are more likely due to similar zinc stearate bridging complexes with different Y ligands [42].

It is noteworthy that these bridging bidentate complexes remain stable after lowering the temperature of ZSO-TME reaction with STA (see experimental Paragraph 2), and that they are absent if the reaction is performed in the presence of C-ZnO-TME.

Thus, it may be suggested that, in ZSO-10, the zinc centers of the amorphous ZnO NPs supported on silica favor the formation of the bridging bidentate complex. In particular, many of these surface zinc centers are linked to silica through Si-O-Zn bond and cannot coordinate four stearate ligands.

The bridging bidentate Zn complex reacts with the accelerator faster than the zinc stearate probably due to its open structure, more easily available to interact with the curatives (stages 2-3 in Scheme 1) than the zinc stearate, where the metal center is coordinated to four bridging carboxylate groups. The formation of this highly reactive intermediate zinc complex may explain the lower apparent activation energy of the induction stage of ZSO-10 and would be in agreement with the Ikeda hypothesis that this species may play a role as active intermediate to accelerate the cross-linking reaction [42].

ATR-FTIR spectra of ZSO and C-ZnO reacted with stearate and successively treated with the accelerator CBS and sulfur at 120°C still show the presence of the bands of both the zinc stearate and the bridging bidentate complex (Figure S6 of Supporting Information). This clearly indicates that the coordination with stearate groups is totally or partially preserved also during reaction with

CBS and sulfur (stage 2-3 in Scheme 1) and the formation of the crosslinking precursors (stage 4). Thus the stearate groups could maintain their coordination also in the active sulfurating Zn accelerator complexes acting as stabilizing ligands and preserving the different structures of the intermediates of ZSO and C-ZnO.

4. Conclusions

In the present study, the catalytic action of silica anchored ZnO, ZSO-10 [20], on the curing of isoprene rubber was investigated in comparison to that of conventional microcrystalline C-ZnO.

The higher curing efficiency of ZSO-10 compared to C-ZnO was explained by its capability to accelerate two stages of the vulcanization process: the formation of the sulfurating complexes at the beginning of reaction and the sulfur network formation.

In fact, the apparent activation energy E_α of the different steps of the vulcanization process, evaluated from DSC, demonstrated that in the induction period of curing the reaction of ZnO with STA and with the other curatives is kinetically favoured in the presence of ZSO-10.

Regarding the sulfur crosslink formation, investigated by MCV, the production of short crosslinking sulfide chains in the cured material was demonstrated to derive from a breaking-down of the longest poly-sulfide chains (S_3-S_8) forming short sulfide chains (S_1, S_2). This desulfuration reaction is faster in the presence of ZSO-10 than with C-ZnO, explaining the higher crosslinking density, calculated by the Flory-Rehner equation, and the better curing efficiency of XZSO-IR composites.

Finally, FTIR analysis suggests that ZSO-10 NPs promote the formation of a stearate bridged bidentate zinc complex $(Zn_2(\mu\text{-}O_2CC_{17}H_{35})_2)^{2+}.4Y$ in the first step of the curing reaction while in the presence of C-ZnO only zinc distearate was detected. The formation of $(Zn_2(\mu\text{-}O_2CC_{17}H_{35})_2)^{2+}.4Y$ was associated to the constraint of tetrahedral geometry around the Zn centers of ZnO bound to silica. This species was suggested to play a key role as highly reactive intermediate in accelerating the cross-linking reaction.

ACKNOWLEDGMENT

This work was in the frame of the European COST action MP1202 “Rational design of hybrid organic-inorganic interfaces: the next step towards advanced functional materials”.

Antonio Susanna and Silvia Mostoni thank CORIMAV (Consortium for the Research of Advanced Materials between Pirelli and Milano-Bicocca University) for its support within the PCAM European Doctoral Program.

Supporting Information

Rheometric parameters of XZSO-IR and M-XZSO-IR; TEM images of ZSO-10; MS spectra of ZSO-TME and of C-ZnO-TME curing products after 10 and 20 minutes of reaction; MS/MS spectra the MCV product TME-S_x-TME with x=1; complete ^{1}H-NMR spectra of C-ZnO-TME and ZSO-TME; ATR-FTIR spectra of pure zinc stearate; ATR-FTIR spectra of ZSO-10 after reaction with STA in the absence of TME; ATR-FTIR spectra in $CHCl_3$ of ZSO-10 and C-ZnO-TME after successive reactions at 120°C with STA; CBS and sulfur. This material is available free of charge via the Internet at http://pubs.acs.org.

References

(1) M. Akiba, A.S. Hashim, Vulcanization and crosslinking in elastomers, Prog. Polym. Sci. 22 (1997) 475-521.

(2)G. Heideman, J.W.M. Noordermeer, R.N. Datta, B. van Baarle, Effect of Zinc Complexes as Activator for Sulfur Vulcanization in Various Rubbers, Rubber Chem. Technol. 78 (2005) 245-257.

(3)A.Y. Coran, Chemistry of the vulcanization and protection of elastomers: A review of the achievements, J. Appl. Polym. Sci. 87 (2003**)** 24-30.

(4) Y. Ikeda, N. Higashitani, K. Hijikata, Y. Kokubo, Y. Morita, M. Shibayama, N. Osaka, T. Suzuki, H. Endo, S. Kohjiya, Vulcanization: New Focus on a Traditional Technology by Small-Angle Neutron Scattering, Macromolecules 42 (2009) 2741-2748.

(5)H. Hirata, in: H. Kondo, Y. Ozawa (Eds.), Chemistry, Manufacture and Applications of Natural Rubber, Woodhead Publishing, Oxford, 2014, pp. 325.

(6)R. Ding, A.I. Leonov, A.Y. Coran, A Study of the Vulcanization Kinetics of an Accelerated-Sulfur SBR Compound, Rubber Chem. Technol. 69 (1996) 81-91.

(7)A.I. Isayev, J.S. Deng, Nonisothermal Vulcanization of Rubber Compounds, Rubber Chem. Technol. 61 (1988) 340-361.

(8)A.P. Mathew, S. Packirisamy, S. Thomas, Studies on the thermal stability of natural rubber/polystyrene interpenetrating polymer networks: thermogravimetric analysis, Polym. Degrad. Stab.72 (2001) 423-439.

(9)M. Tiwari, J.W.M. Noordermeer, W.K. Dierkes, W.J. van Ooij, Effect of Plasma Polymerization on the Performance of Silica in NBR, EPDM and NBR/EPDM Blends, Rubber Chem. Technol. 81 (2008) 276-296.

(10) N.J. Morrison, M. Porter, Temperature Effects on the Stability of Intermediates and Crosslinks in Sulfur Vulcanization, Rubber Chem. Technol. 57 (1984) 63-85.

(11) A.Y. Coran, Chapter 7, in: F.R. Eirich (Ed.), Science and Technology of rubber, Academic Press, New York, 1978.

(12) A.Y. Coran, Vulcanization. Part V. The Formation of Crosslinks in the System: Natural Rubber-Sulfur-MBT-Zinc Ion, Rubber Chem. Technol. 37 (1964) 679-688.

(13) K. Fujimoto, K. Wataya, The study of polymers by high-temperature ATR spectroscopy, J. Appl. Polym. Sci. 13 (1969) 2513-2526.

(14) J.H.M. Van De Berg, J.W. Beulen, E.F.J. Duynstee, H.L. Nelissen, Model Vulcanization of EPDM Compounds—Part I: Structure Determination of Vulcanization Products from Ethylidene Norbornane, Rubber Chem. Technol. 57 (1984) 265-274.

(15) A.V. Chapman, The influence of excess zinc stearate on the chemistry of sulfur vulcanization of natural rubber, Phosphorus, sulfur, and silicon and the related elements 59 (1991) 565-568.

(16) M.R. Krejsa, J.L. Koenig, A Review of Sulfur Crosslinking Fundamentals for Accelerated and Unaccelerated Vulcanization, Rubber Chem. Technol. 66 (1993) 376-410.

(17) P. Versloot, J.G. Haasnoot, P.J. Nieuwenhuizen, J. Reedijk, M. van Duin, J. Put, Sulfur Vulcanization of Simple Model Olefins, Part V: Double Bond Isomerization during Accelerated Sulfur Vulcanization as Studied by Model Olefins, Rubber Chem. Technol. 70 (1997) 106-119.

(18) B. Simon-Hettich, Environmental Health Criteria 221 Zinc, in: A. Wibbertmann, D. Wagner, H. Malcolm, Environmental Health Criteria 221 (WHO), World Health Organization, Geneva, 2001, pp. 195.

(19) A.G. Heath, Uptake, Accumulation, Biotransformation and Excretion of Xenobiotics, in: A.G. Heath (Ed.), Water Pollution and Fish Physiology, 2nd ed., Lewis, 1995, pp. 82.

(20) A. Susanna, L. Armelao, E. Callone, S. Dirè, M. D'Arienzo, B. Di Credico, L. Giannini, T. Hanel, F. Morazzoni, R. Scotti, ZnO nanoparticles anchored to silica filler. A curing accelerator for isoprene rubber composites, Chem. Eng. J. 275 (2015) 245-252.

(21) S.V. Vyazovkin, A.I. Lesnikovich, An Approach to the solution of the inverse kinetic problem in the case of complex process. Part I methods employing a series of thermoanalytycal curves, Thermochim. Acta 165 (1990) 273-280.

(22) S.V. Vyazokin, V.I. Goryachko, A.I. Lesnikovich, An approach to the solution of the inverse kinetic problem in the case of complex processes: Part III Parallel indipendent reactions, Thermochim. Acta 197 (1992) 41-45.

(23) F.K. Lautenschlaeger, K. Edwards, Model Compound Vulcanization—Part V. The Effect of Chemical Additives and Fillers, Rubber Chem. Technol. 53 (1980) 27-47.

(24) S. Rodriguez, C. Masalles, N. Agullo, S. Borros, L. Comellas, F. Broto, Identification of the Intermediates Sulfur Vulcanization of Natural Rubber, Kautschuk Gummi Kunststoffe 52 (1999) 38-445.

(25) M. Geyser, W.J. McGill, Thiuram-accelerated sulfur vulcanization. II. The formation of crosslink precursors, J. Appl. Polym. Sci. 60 (1996) 431-437.

(26) M. Geyser, W.J. McGill, Thiuram-accelerated sulfur vulcanization. I. The formation of the active sulfurating agent, J. Appl. Polym. Sci. 60 (1996) 425-430.

(27) P.J. Nieuwenhuizen, S. Timal, M.J. v. Veen, J.G. Haasnoot, J. Reedijk, Homogeneous Zinc(II) Catalysis in Accelerated Vulcanization I. Reaction-Stage Modeling and Cross-Link Formation, Rubber Chem. Technol. 71 (1998) 750-765.

(28) R.T.S. Monticone, A.V. Kanaev, Complex Nature of the UV and Visible Fluorescience of Colloidal ZnO Nanoparticles, J. Phys. Chem. B 102 (1998) 2854-2862.

(29) B. Ellis, G.N. Welding, Estimation, from Swelling, of the Structural Contribution of Chemical Reactions to the Vulcanization of Natural Rubber.Part II. Estimation of Equilibrium Degree of Swelling, Rubber Chem. Technol. 37 (1964) 571-575.

(30) P.J. Flory, J. Rehner, Statistical Mechanics of Cross─Linked Polymer Networks II. Swelling., J. Chem. Phys. 11 (1943) 521-526.

(31) P.J. Flory, J. Rehner, Thermodynamics of High Polymer Solutions, J. Chem. Phys. 10 (1942) 51-61.

(32) R. Orwoll, P. Arnold, Polymer–Solvent Interaction Parameter χ, in: J. Mark (Ed.), Physical Properties of Polymers Handbook, Springer, New York, 2007, pp. 233-257.

(33) H.E. Kissinger, Reaction Kinetic in Differencial Thermal Analysis, Anal. Chem. 29 (1957) 1702-1705.

(34) B.V.M. Guzman, N. Agullo, U. Giese, S. Borros, Zinc Oxide Versusus Magnesium Oxide Revisited. Part I, Rubber Chem. Technol. 85 (2012) 38-55.

(35) J. Flynn, L. Wall, General treatment of the thermogravimetry of polymers, J. Res. Nat. Bur. Stand.. Section A. Physics and chemistry 70 (1966) 487-523.

(36) M. Lopez Manchado, M. Arroyo, B. Herrero, J. Biagiotti, Vulcanization kinetics of natural rubber-organoclay nanocomposites, J. Appl. Polym. Sci. 89 (2003) 1-15;

(37) S. Rabiei, A. Shojaei, Vulcanization kinetics and reversion behavior of natural rubber/styrene butadiene rubber blend filled with nanodiamond - the role of sulfur curing system, Euro. Polym. J. 81 (2016) 98-113.

(38) P.J. Nieuwenhuizen, J.G. Haasnoot, J. Reedijk, Homogeneous Zinc(II) Catalysis in Accelerated Vulcanization II. (Poly)Olefin Oxidation, Dehydration, and Reaction with Anti-Reversion Coagents, Rubber Chem. Technol. 72 (1999) 15-26.

(39) G. Heideman, R.N. Datta, J.W.M. Noordermeer, Activators in accelerated sulfur vulcanization, Rubber Chem. Technol. 77 (2004) 512-541.

(40) P.J. Nieuwenhuizen, M.J. v. Veen, J.G. Haasnoot, J. Reedijk, Homogeneous Zinc(II) Catalysis in Accelerated Vulcanization IV. The mechanism of cross-link (de)sulfuration, Rubber Chem. Technol. 72 (1998**)** 43-54.

(41) M.G. Fonseca, A.S. Olivera, C. Airoldi, Silylating Agents Grafted onto Silica Derived from Leached Chrysotile, J. Colloid Interface Sci. 240 (2011) 533-538.

(42) Y. Ikeda, Y. Yasuda, T. Ohashi, H. Yokohama, S. Minoda, H. Kobayashi, T. Honma, Dinuclear Bridging Bidentate Zinc/Stearate Complex in Sulfur Cross-Linking of Rubber, Macromolecules 48 (2015) 462-475.

(43) G. Schürer, T. Clark, R. v. Eldik, in: Z. Rappoport, I. Marek (Eds.), The Chemistry of Organozinc Compounds, John Wiley Sons Ltd., London, 2006, pp 31.

(44) D. Dutta, S. Mishra, The structural and energetic aspects of substrate binding and the mechanism of action of the DapE-encoded N-succinyl-l,l-diaminopimelic acid desuccinylase (DapE) investigated using a hybrid QM/MM method, Phys. Chem. Chem. Phys. 16 (2014) 26348-26358.

(45) T. Ishioka, Y. Shibata, M. Takahashi, I. Kanesaka, Vibrational spectra and structures of zinc carboxylates II. Anhydrous zinc acetate and zinc stearate, Spectrochim. acta. Part A 54A (1998) 1811-1818.

(46) V. Zeleňák, Z. Vargová, K. Györyová, Correlation of infrared spectra of zinc(II) carboxylates with their structures, Spectrochim. acta. Part A 66A (2007) 62-272.

(47) C.C.R. Sutton, G.D. Silva, G.V. Franks, Modeling the IR spectra of aqueous metal carboxylate complexes: correlation between bonding geometry and stretching mode wavenumber shifts, Chem. Eur. J. 21 (2015) 6801-6805.